Bayesian Combined Active/Passive (B-CAP) Soil Moisture Retrieval Algorithm

Matias Barber, *Member, IEEE*, Cintia Bruscantini, *Member, IEEE*, Francisco Grings, and Haydee Karszenbaum, *Member, IEEE*

***Abstract*—This paper focused on exploiting remotely sensed active and passive observations over agricultural fields for soil moisture retrieval purposes. Co-polarized backscattering coefficients HH and VV and V-polarized brightness temperature T_{bV} measurements were merged onto a Bayesian algorithm to enhance field-based retrieval estimates. The Bayesian algorithm relies on the use of active SAR to constrain passive information. It is assumed that observations are representative of an extent involving field sizes of about 800 m by 800 m, disregarding the scaling issues between the high resolution SAR pixel and the coarse resolution passive pixel. The integral equation model with multiple scattering at second order (IEM2M) and the $\omega - \tau$ model were used as forward models for the backscattering coefficients and for the V-polarized brightness temperature, respectively. The Bayesian algorithm was assessed using datasets from the Soil Moisture Active Passive Validation Experiment 2012 (SMAPVEx12). Such datasets are representative of contrasting soil conditions since soil moisture spanned almost its whole feasible range from 0.10 to 0.40 cm^3/cm^3, at different observation geometries with incidence angles ranging from 35° to 55°. Also, the fairly large amount of measurements (97) made the dataset complete for assessment purposes. Soil moisture variability at field scale and dielectric probe error were accounted for in the comparison between retrieved estimates and *in situ* measurements. Performance metrics were used to quantify the agreement of the retrieval methodology to *in situ* information, and to assess the improvement in the combined methodology with respect to the single ones (active or passive). Overall, the root mean squared error (RMSE) showed an improvement from 0.08 to 0.11 cm^3/cm^3 (only active) or 0.03–0.12 cm^3/cm^3 (only passive, after bias correction) to 0.06–0.10 cm^3/cm^3 (combined), thus, demonstrating the potential of such combined soil moisture estimates. When analyzed each field separately, RMSE is less than 0.07 cm^3/cm^3 and correlation coefficient r is greater than 0.6 for most of the fields.**

***Index Terms*—Bayes procedures, inverse problems, moisture, radar applications, remote sensing, rough surfaces, soil measurements, synthetic aperture radar (SAR).**

I. Introduction

ON-GOING and near-future synthetic aperture radar (SAR) satellite missions are expected to provide meaningful and timely information about soil condition over vast agricultural lands such as those of the mid-western United States (corn-belt) and of Argentina (Pampas Plain), leading to actual economic benefits regarding to seeding dates, irrigation strategies, and crop yield forecasting. NASA's soil moisture active and passive (SMAP) [1] and Argentinean SAOCOM (www.conae.gov.ar) missions have been specifically designed to develop surface soil moisture products. These missions will exploit microwave radar at L-band ($\lambda = 23$ cm) as sensing wavelength, which was demonstrated to be less sensitive to residue cover over soil's surface and to be more accurate on retrieving soil moisture than other bands. The relevance of this study relies on the on-going satellite L-band missions (ALOS-2, SMAP) enhanced by the forthcoming SAOCOM and the planned DLR TanDEM-L [2] missions.

SAR systems offer the added advantages of fine resolution (on the order of 10 m), multiple polarimetric modes, and a variety of beam incidence angles, which make them unique to develop soil moisture products over agricultural lands. However, modeling the scattering processes that relate backscattering coefficient σ^0 to soil properties (moisture and roughness) is hampered by the speckle noise [3] and the difficulty in measuring soil roughness in the field [4]. The former mainly relates to the SAR imaging system, whereas the latter relates to the heterogeneity of soil properties. Moreover, several combinations of soil surface parameters can often lead to the same SAR observation. Thus, the impact of soil heterogeneity on retrieving soil moisture from SAR should be somehow minimized. In effect, agricultural lands are often divided into smaller fields, each one characterized by the same land management and land use over several growing seasons. Therefore, these fields usually have the lowest variability of soil properties in relation with larger areas. In this way, estimates defined on a field basis are best suited for SAR-based retrieval purposes.

Information from passive remote sensing can also be used to aid to constrain the retrieval of soil moisture. Microwave emissions are more strongly correlated to soil dielectric properties than active SAR, but can only be collected at coarser resolution (40 km in case of SMAP). Soil emissivity (passive microwave) and soil reflectivity (active microwave) are correlated, i.e., thermal microwave emission (brightness temperature) decreases and backscattering cross section (backscattering coefficient) increases in response to an increase in the dielectric constant (due to soil moisture) from the land surface, respectively. However, joint models in which soil emissivity and reflectivity are modeled under the same physical basis (usually energy conservation principle) are very complex ones to be used in an operational retrieval algorithm, even in the simplest case of bare soil.

Manuscript received March 8, 2016; revised July 8, 2016 and September 1, 2016; accepted September 14, 2016. Date of publication October 4, 2016; date of current version November 30, 2016. This work was supported by the National Scientific and Technical Research Council. (*Corresponding author: Matias Barber.*)

The authors are with the Institute of Astronomy and Space Physics, Quantitative Remote Sensing Group, Buenos Aires C1428ZAA, Argentina (e-mail: mbarber@iafe.uba.ar; bruscantinica@gmail.com; verderis@iafe.uba.ar; haydeek@iafe.uba.ar).

Color versions of one or more of the figures in this paper are available online at http://ieeexplore.ieee.org.

Digital Object Identifier 10.1109/JSTARS.2016.2611491

This paper addresses these different issues in the context of a Bayesian retrieval scheme. Within this frame, the above discussion leads to the following remarks:

1) The choice of forward models, for both the active and passive microwaves, should respond to simplicity and ease of use in the retrieval algorithm (i.e., lesser number of ancillary data and model parameters suited for remotely sensed observations).
2) A large-scale soil moisture guess from passive microwaves can be used to constrain the active information included in the likelihood.
3) Through inversion of the passive forward model, the guess soil moisture is an average of the actual soil moisture within the footprint of the radiometer. The lower the heterogeneity in soil moisture of the fields encompassing the pixel, the lesser the errors due to biased priors. Situations with high heterogeneity in soil moisture should be carefully evaluated and they are out of the scope of this paper. Disaggregation algorithms were developed to downscale coarse resolution radiometer data into an intermediate product by means of SAR data [5], this way minimizing the incidence of heterogeneity in the guess estimate. However, this intermediate radiometer data might be highly correlated to SAR data.

Ideally, a Bayesian Combined Active/Passive (B-CAP) retrieval algorithm yields the smaller errors when active and passive information is collected at similar spatial resolution (for instance, using data from an airborne campaign).

Previous studies employing Bayesian merging techniques adopt Gaussian distributions to include the speckle noise and the model errors [6], [7]. However, when dealing with polarimetric data with small number of looks or when the shape of the posterior is wanted to be estimated accurately, a better modeling of the speckle noise is needed. The shape of the posterior, which is related to the forward model chosen, the error sources considered (speckle noise, model or instrument errors, etc.), and the contextual information, furnishes information about the entire process of a rough, dielectric surface being observed by a SAR sensor and the uncertainty about the soil parameters. One of the distinctive aspect of the methodology presented in this paper is that the residual speckle noise after multilooking is modeled using the exact distribution for a bivariate intensity-pair image.

Low resolution radiometer data has been combined with high resolution SAR data using the radar backscatter spatial patterns within the radiometer footprint to disaggregate the radiometer brightness temperature [8]. This method is used as baseline SMAP algorithm [9] and was recently evaluated using airborne active and passive observations in a diverse agricultural region [10]. Other combined active/passive (CAP) approaches involve joint-physics [11] where optimum model parameters, which minimize an unified cost function of the active and passive data, are recorded as retrieved soil moisture [11], the use of SAR to determine the relative amount of change in soil moisture within the footprint of a radiometer through a time series analysis [12], and SMAP optional algorithms: T_b disaggregation at high (3 km) and medium (9 km) resolutions [9].

In a recent paper [13], microwave radiometer observations from Soil Moisture Active Passive Validation Experiment 2012 (SMAPVEx12) field experiment data has been exploited to estimate soil moisture. This soil moisture retrieval is based on L-band brightness temperature, where a correction for the rough surface reflectivity is defined and tuned for different soil texture conditions. This reflectivity correction depends on soil moisture level and the proximity of the last rain event. Therefore, this retrieval algorithm needs a number of ancillary data such as soil texture (to estimate wilting point and field capacity) and precipitation occurrence (to estimate the number of days since the last precipitation event) whose availability may be limited in large croplands.

Validation of field-based retrieved estimates against ground-truth data should be done carefully, since different spatial scales are involved. On the one hand, retrieved estimates represent mean soil moisture over a spatial domain defined by the outer limits of the field, typically ranging from 1 to 50 ha. On the other hand, soil moisture estimates derived from ground-based sampling involve a finite (and often small) number of point measurements (over an extent of 1 m $\times$ 1 m) performed with nonideal (i.e., with errors) instruments. Since agricultural fields are regarded as the unit for retrieving purposes, field-intrinsic soil moisture variability should be taken into account. This variability cannot be measured from a high resolution SAR image over the agricultural field, due to radiometric uncertainties from speckle noise. It only can be estimated by means of a field experiment (see, for example, Famiglietti *et al.* [14]). This variability becomes critical when comparing the performance of retrieved estimates against ground-truth data [15]. Despite this, and to the authors knowledge, errors in ground-based estimates are usually disregarded. Accounting for the errors in the ground-truth data due to the well-known spatial variability of soil moisture constitutes another distinctive aspect in this paper.

We present here a Bayesian active/passive methodology in which soil moisture estimations from passive microwave data are used to constrain the estimation from active radar ones through a preliminary soil moisture guess (through a single channel algorithm (SCA)), providing active and passive observations correspond to similar field extents. This methodology exploits outstanding IEM2M as forward model [16] to describe radar rough-surface scattering of bare or sparsely vegetated soils and can be used to test SMAP active/passive soil moisture product in bare soils over agricultural lands. The capability of passive microwave measurements to improve radar soil moisture predictions is demonstrated in this paper with *in situ* and airborne observations from the SMAPVEx12 field campaign.

II. Dataset Description

A. Site Description and Airborne Instruments (UAVSAR and PALS)

The dataset to test the Bayesian approach were taken from the SMAPVEx12 over southwest of Winnipeg, Manitoba, Canada. The reader is referred to [17] and [18] for a complete description of the dedicated field campaign. Seventeen bare and sparsely vegetated soybean fields were chosen. Soybean fields were

imaged by NASA/JPL's Uninhabited Aerial Vehicle Synthetic Aperture Radar (UAVSAR) and by Passive Active L-band System (PALS) every 2–3 days during a six-week campaign from June 7 to July 19. Because of the different acquisition dates, fields were imaged several times during the campaign. Moreover, each acquisition of the UAVSAR was comprised of four main flight lines, namely 31603, 31604, 31605, and 31606, with different incidence angles.

UAVSAR provided fully polarimetric L-band imagery at beam incidence angles comprising 20–60° due its right-looking antenna at a nominal incidence angle of 40°. It acquires backscattering coefficients HH, HV, and VV at a frequency of 1.26 GHz with absolute radiometric calibration bias better than 1 dB and residual root-mean-square (RMS) errors of ∼0.7 dB [19]. The pixel size on the ground projected image is 5.00 m × 7.20 m. Multilooking of the pixels within a field leads to a backscattering coefficient related to an area of about 800 m by 800 m (field size).

PALS was mounted at a 40° incidence angle looking to the rear of the aircraft, so that a 40° nominal incidence angle was fixed throughout the images. It acquires H- and V-polarized brightness temperatures at a frequency of 1.413 GHz with uncertainties of 1 K (bias) and 0.2 K (stability) [20]. The flight altitude was about 2600 m above ground level with an effective spatial resolution of about 900 m by 1600 m (see [17, Table 3]). Co-located surface soil temperature using an infrared camera attached to the aircraft was also measured.

The brightness temperature T_b were spatially collocated by averaging those PALS measurements that felt within each field. The low-altitude radiometer footprint size was approximately 500 m and T_b was acquired over separate flight lines which did not cover all the fields. For this reason some fields had not their corresponding T_b measurement. It is also important to note that PALS provides a single beam of data along a flight track and that any mapping must rely upon multiple flight lines at a spacing of the footprint width.

Concurrent with the airborne acquisitions, *in situ* soil moisture (0–6 cm) was collected using handheld probes. Each field was sampled at $N=16$ locations along two transects across the field. At each location, $M=3$ replicates were measured. Additional soil and vegetation characterization took place on the non-flight days during the campaign: roughness RMS height s and correlation length l, soil texture (sand S and clay C contents) and vegetation water content VWC.

B. Preprocessing

Agricultural lands are often divided into smaller fields each one characterized by the same land management and land use over several growing seasons. Thus, it is appropriate to assume that those fields are the larger agricultural extents in which land properties can be regarded as homogeneous. The relevance of this consideration is twofold: first, it sets the maximum average window over which neighboring pixels can be average to reduce the impact on radiometric uncertainties due to speckle noise, leading to a definite (i.e., with low variance) backscattering coefficient. Second, accurate remotely sensed soil moisture estimates arise from a definite backscattering coefficient. For this reason, SAR-based soil moisture estimates are best defined on a field basis. These estimates will be referred to as "field-based retrieved estimates" hereafter.

For each field, the number of looks n was computed as follows. First, image is multilooked averaging pixels within squares of increasing size (2 × 2, 3 × 3, and so on). Then, the sample variance of the backscattering coefficient from each multilooked images is computed. When the variance is not decreased as the number of looks increased, the corresponding $n=\mu^2/\mathrm{var}$ is used, where μ is the mean value and var the variance for HH. In other words, the speckle effect is reduced until the heterogeneity of the scatter dominates the variance of the target. The rationale behind this procedure is that it is meaningless to multilook an image beyond the intrinsic heterogeneity of the underlying scatter, since the resulting n will be overestimated. Thus, the number of looks takes into account the residual speckle as well as the heterogeneity of the underlying scatter. At this step, the mean values ($\mathrm{HH}_{\mathrm{meas}}, \mathrm{VV}_{\mathrm{meas}}$) of the backscatter coefficients and the correlation ρ between HH and VV channels are also computed.

III. Overview of the CAP Bayesian Approach

A. Bayesian Theorem in the Context of SAR Products

The Bayesian approach presented here is based on the bivariate version of the Bayes' theorem. An expression for the conditional ("posterior") probability of measuring a certain set of soil parameters (ε and s) given measurements of backscattering coefficients z_1 and z_2 can be obtained from Bayes' theorem:

$$P(\varepsilon, s|z_1, z_2) = \frac{P_{Z_1 Z_2}(z_1, z_2|\varepsilon, s) P_{\mathrm{ES}}(\varepsilon, s)}{P_{Z_1 Z_2}(z_1, z_2)} \tag{1}$$

where $P_{Z_1 Z_2}(z_1, z_2|\varepsilon, s)$ is the probability of measuring a certain set (z_1, z_2) of backscattering coefficients given measurements of soil dielectric constant ε and RMS height s (the "likelihood function"), P_{ES} is the prior joint density function of ε and s and $P(z_1, z_2)$ (the "evidence") is a global normalizing factor and it is the probability of a certain set (z_1, z_2) to be measured. The likelihood function is a stochastic version of the forward model and measures the degree of compatibility between a certain SAR measurement and certain soil parameters constrained to some given forward model. The higher the values of the likelihood, the more likely that the SAR measurement come from that specific combination of soil parameters, provided an error-free model is available. The likelihood takes into account the forward model as well as the speckle noise and therefore its spread is due to soil parameter sensitivity and the speckle noise [21]. The prior involves all the information available about soil parameters ε and s. It can be available from historical records, estimation from other sensors, *in situ* data and/or contextual information. With the likelihood and the prior at hand, the posterior is computed by a point-by-point product of them.

Then, providing the conditional density function (1) is exact, the optimal unbiased estimator for the mean value of ε that has

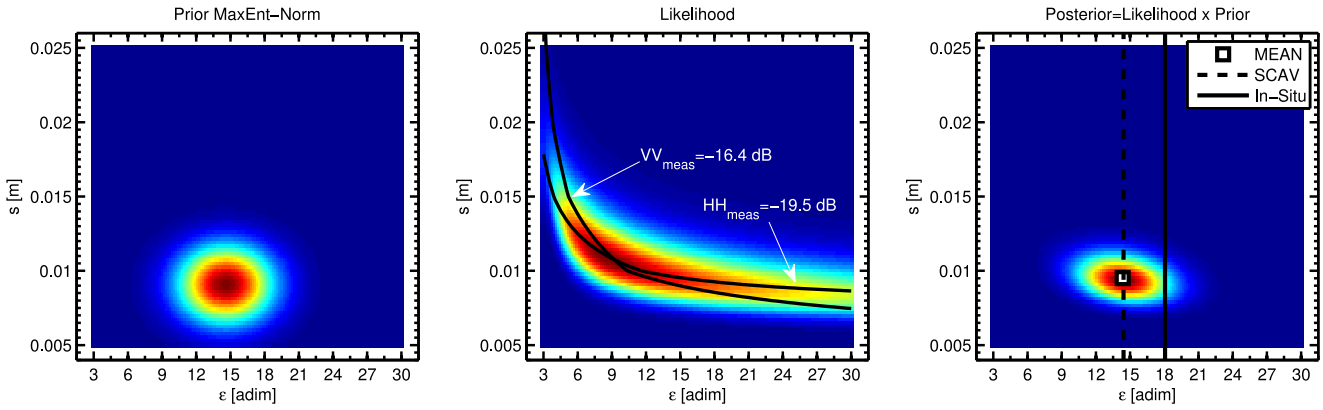

Fig. 1. Posterior as the product of the prior and the likelihood. The prior is assumed to be constructed with information from passive microwaves. The likelihood spans the region where the measured backscattering coefficients are compatible to residual speckle noise and heterogeneities within the target. The mean estimator $\varepsilon^{\mathrm{bay}}$, the SCA for V-polarized brightness temperature estimator SCAV and the *in situ* estimator for real dielectric constant are indicated on the posterior.

the minimum variance is the mean of (1)

$$\varepsilon^{\mathrm{bay}} = \iint_D \varepsilon P\left(\varepsilon, s|z_1, z_2\right) d\varepsilon ds \tag{2}$$

and similarly the squared standard deviation std$[\cdot]$ of this estimator is

$$\mathrm{std}[\varepsilon^{\mathrm{bay}}]^2 = \iint_D (\varepsilon - \varepsilon^{\mathrm{bay}})^2 P\left(\varepsilon, s|z_1, z_2\right) d\varepsilon ds \tag{3}$$

where an explicit expression for (1) must be found in order to calculate $\varepsilon^{\mathrm{bay}}$ and its standard deviation. The integration domain D in (2) and (3) spans the same validity range than the forward model with respect to (ε, s). The standard deviation std$[\varepsilon^{\mathrm{bay}}]$ can be used as a measure of the error of the retrieved estimate $\varepsilon^{\mathrm{bay}}$. In addition, a number of error metrics will be used to assess the performance of the retrieved estimates against ground-truth data [22] (e.g., maximum absolute error, MAE; root mean squared error, RMSE; bias, *b*; unbiased-RMSE, ubRMSE; and sample correlation, *r*).

B. Posterior

The posterior is built as the product of the likelihood function by the prior distribution as shown in Fig. 1. Dielectric constant estimates are computed from the posterior distribution as mentioned in Section III-A, and then converted into soil moisture using the empirical relationship described further in Section IV-D. Measured backscattering coefficients $\mathrm{HH}_{\mathrm{meas}}$ and $\mathrm{VV}_{\mathrm{meas}}$ are shown on the likelihood as contours. Residual speckle noise on intensity images and heterogeneity of the backscatter enlarges the region on the space (ε, s) compatible to measured coefficients $\mathrm{HH}_{\mathrm{meas}}$ and $\mathrm{VV}_{\mathrm{meas}}$.

C. Likelihood Function Construction

Let be assumed that co-polarized backscattering coefficients are at hand, i.e., $(Z_1, Z_2) = (\mathrm{HH}, \mathrm{VV})$, so that $(z_1, z_2) = (\mathrm{hh}, \mathrm{vv})$. The likelihood function is constructed as follows. First, the validity range of a forward model, referred to as C, in terms of ε and s is discretized (for a fixed wavelength, see Section IV-A). The remaining parameters, (correlation length l, incidence angle θ, and wavelength λ) will be assumed to be known, either by ground-based measurements (l) or by the sensor parameters (θ, λ). Second, each pair (ε, s) is converted to backscattering coefficient throughout the forward model $C(\varepsilon, s, l; \theta, \lambda)$, leading to a grid of pairs $(\mathrm{hh}, \mathrm{vv})$ which represents the backscattering properties of the target. The variance due to speckle noise of the expected value of $(\mathrm{HH}, \mathrm{VV})$ is modeled by means of the bivariate gamma distribution $P_{\mathrm{HHVV}}(\mathrm{hh}, \mathrm{vv}|C_{\mathrm{HH}}, C_{\mathrm{VV}}, n, \rho)$, as explained in Section IV-B. Thus, each pair (ε, s) is associated to a bidimensional bivariate distribution $P_{\mathrm{HHVV}}(\mathrm{hh}, \mathrm{vv}|\varepsilon, s; l, \theta, \lambda, n, \rho)$ throughout the forward model $C_i(\varepsilon, s, l; \theta, \lambda)$, $i = \mathrm{HH}, \mathrm{VV}$. This is the likelihood function. By using the procedure described in Section II-B, the likelihood spreads on an area onto the (ε, s)-space which takes into account the model uncertainties as well as the residual speckle noise at the same time.

D. Prior Distribution

The prior distribution describes the possible values of soil dielectric constant ε and RMS height s before SAR acquisition takes place. In what follows, it will be assumed independence between ε and s, i.e., $P_{\mathrm{ES}}(\varepsilon, s) = P_E(\varepsilon) P_S(s)$. Two kinds of priors are taken into account. When passive microwave-based soil moisture guess is not available, an uniform prior $P_E \sim U(3, 30)$ for ε is used instead. A normal distribution is used to describe the uncertainty around the mean value μ_s of the ground-based estimate s. Mathematically, $P_S \sim N(\mu_s, \sigma_s)$. The uncertainty σ_s is arbitrarily set to $0.20\,\mu_s$.

When passive microwave observations are available, they enable the use of soil moisture estimations from the brightness temperature of the soil as the prior $P_E(\varepsilon)$. The $\omega - \tau$ model [9], [23] is a rather simple physical model used to link the observed brightness temperature (T_b) with surface dielectric and geometric properties. The $\omega - \tau$ model is of the form

$$T_{\mathrm{bV}} = T_S(1 - r_v)e^{-\frac{\tau}{\cos\theta}} + T_C(1 - \omega)(1 - e^{-\frac{\tau}{\cos\theta}})(1 + r_v e^{-\frac{\tau}{\cos\theta}}) \tag{4}$$

where T_S and T_C are the soil surface and vegetation temperature, respectively (that will be assumed equal), r_v is the reflectivity, τ represents the optical depth, and is b parameter multiplied by vegetation water content (VWC, [kg/m^2]), and θ is the incidence angle. For the soybeans fields analyzed here, vegetation parameter b was set to be 0.13 based on [24, Table I]. Vegetation water content was derived from plant water content obtained from *in situ* measurements [18]. Vegetation scattering parameter ω was set to 0.05 following again [24, Table I].

The $\omega - \tau$ is readily invertible by means of the SCA [25]. Thus, the estimated dielectric constant from passive V-polarized brightness temperature T_{bV} is used to center a Maximum Entropy (MaxEnt) probability distribution into the prior. The main advantage of the MaxEnt statistical inference is the absence of any external hypothesis other than the mean and the upper and lower bound of the range. One way to generate such a MaxEnt probability distribution subject to these constraints is to use Lagrange multipliers [26]. The lower and upper bound for the dielectric constant was $\varepsilon_{\min} = 3$ and $\varepsilon_{\min} = 30$, respectively. Error sources in SCA are mainly related to the uncertainties on the brightness temperature and to the estimation of soil and vegetation temperature from infrared camera on board PALS.

IV. CAP Bayesian Algorithm

A. Forward Model

The integral equation model with multiple scattering at second order, named as IEM2M [16], is the name given to an improved, enhanced version of the integral equation model originally developed by Fung [27] to describe rough-surface scattering in the field of radar remote sensing for Earth observation. The backscattering coefficient in the IEM2M formulation can be written as the sum of a single scattering term and a multiple scattering term

$$\sigma^0_{\rm qp} = \sigma^0_{\rm qp}(S) + \sigma^0_{\rm qp}(M) \tag{5}$$

where $\sigma^0_{\rm qp}(S)$ is the single scattering term, $\sigma^0_{\rm qp}(M)$ is the multiple scattering term, and the subscripts q, p state for the receiving and transmitting polarizations, respectively. The single scattering term $\sigma^0_{\rm qp}(S)$ accounts for the electromagnetic radiation that leaves the rough surface after only one interaction with its interface. This is a local phenomenon and depends only on the contact point between the radiation and the surface. Conversely, radiation that have multiple interactions at the interface is accounted for in $\sigma^0_{\rm qp}(M)$. This latter is not a phenomenon merely local as depends on the entire configuration of the rough surface. Mathematically, the single scattering term $\sigma^0_{\rm qp}(S)$ corresponds to terms fully integrated, which are readily evaluated, whereas $\sigma^0_{\rm qp}(M)$ involves a number of high-dimensional integrations [16].

Since IEM2M is based on Kirchhoff approximation, its validity range in terms of RMS height s, correlation length l, and wavenumber k ($= \frac{2\pi}{\lambda}$) is [28], [29]

$$k\frac{l^2}{2\sqrt{3}s}\left(1+\frac{2s^2}{l^2}\right)^{3/2} \gg 1 \tag{6}$$

which physically implies a large local radius of curvature.

To avoid multiple scattering calculations (which requires at least a four-dimensional integration) found in the term $\sigma^0_{\rm qp}(M)$, further approximations are made in order to numerically evaluate expression (5) so that $\sigma^0_{\rm qp} \approx \sigma^0_{\rm qp}(S)$. The term $\sigma^0_{\rm qp}(M)$ can be neglected under the following conditions [30]:

$$ks < 2 \tag{7a}$$

$$s/l < 0.3. \tag{7b}$$

Care was taken to perform the retrieval only using measurements that agreed with conditions (6) and (7).

A pre-requisite for the use of a theoretical model is the validation of the model against the field measurements and related backscattering coefficients. First, IEM2M validity range were checked using (6). Measurements where pairs (s, l) yield (6) greater than 3 were kept. Second, it turned out that measurements with quite small and quite large incidence angle were poorly described by the IEM2M. Thus, only measurements between $\theta = 35°$ and $\theta = 55°$ were kept. Finally, since IEM2M assumes bare or sparsely vegetated soil, Radar Vegetation Index (RVI) [31] was used to characterize the vegetation volume scattering. Thus, fields with low RVI (RVI < 0.3) were assumed to behave as a bare soil at L-band. Model prediction against observations is shown in Fig. 2 for the measurements that fulfilled inequation (6) larger than 3, incidence angle $35° < \theta < 55°$, and RVI < 0.3. The IEM2M models reasonably well the dataset, where contrasting soil conditions were presented. Fields are color-coded and indicated with text arrows. Some similar studies comparing IEM model simulations and remotely sensed radar measurements at L-band reported errors ranging from 2 [32] to 3–5 dB [33].

Microwave backscattering from a random surface is monotonically increasing with dielectric constant ε and roughness s. Also, HH and VV backscattering coefficients have different sensitivities to soil moisture, so that the larger the soil moisture, the greater the difference between HH and VV. The same holds for soil roughness. Thus, since soil roughness is considered to remain stationary over time for each field, the difference between measured HH and VV is related to soil moisture.

The effect of model overestimation on the predicted soil moisture can be understood as follows. Let be assumed that a pair $(\mathrm{HH}_{\rm meas}, \mathrm{VV}_{\rm meas})$ is observed. These backscattering coefficients correspond to a surface with actual (ε, s) provided the model is accurate (i.e., no model errors). If the model overestimates the measured $(\mathrm{HH}_{\rm meas}, \mathrm{VV}_{\rm meas})$, it follows that smaller (ε, s) will reproduce the observed backscattering coefficients via the inaccurate model. Roughly speaking, fields 63, 111, and 113 for acquisition 31605, and fields 103 and 113 for acquisition 31606 are expected to underestimate *in situ* soil moisture. Conversely, field 14 for acquisition 31606 is expected to overestimate *in situ* soil moisture since for this field model prediction underestimates observed backscattering coefficient. Since no model biases were accounted for in the simulation, the likelihood spreads around the intersection of the level curves given by $(\mathrm{HH}_{\rm meas}, \mathrm{VV}_{\rm meas})$. However, the intrinsic heterogeneity of

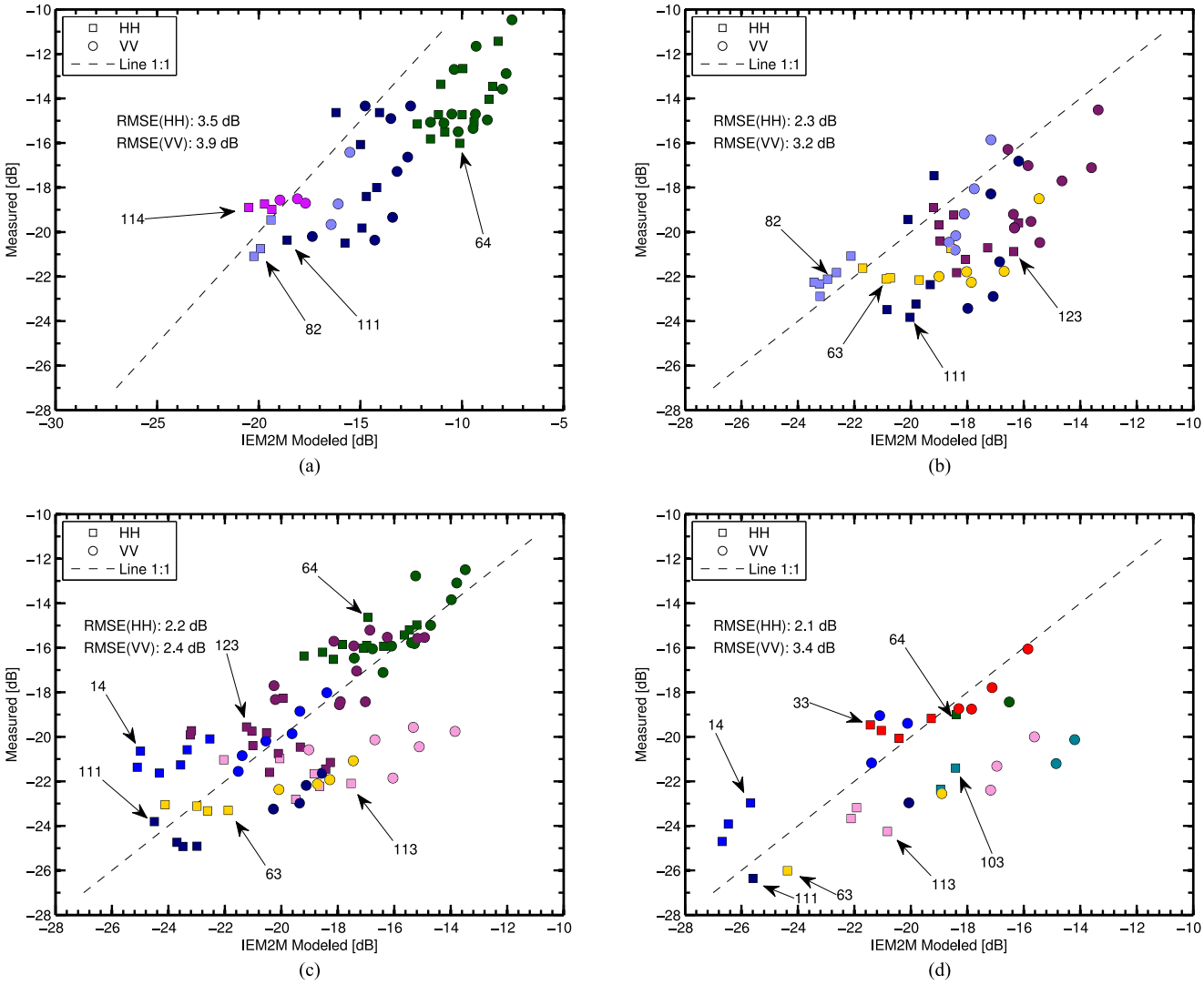

Fig. 2. IEM2M model validation against field measurements for HH and VV backscattering coefficients. Data were collected from four different UAVSAR flight lines (31603–31606) on different acquisition dates. Dataset were selected among those (s,l) pairs for which (6) is larger than 3, incidence angle $35° < \theta < 55°$, and RVI < 0.3. Fields are color-coded and indicated with text arrows. (a) Flight line 31603. (b) Flight line 31604. (c) Flight line 31605. (d) Flight line 31606.

the underlying scatter is taken into account by the number of looks since the average standard deviation of the backscattering coefficients is about the RMSE shown in Fig. 2.

B. Speckle Noise

The estimator derived from the stochastic (Bayesian) procedure described in Section III-A is affected by speckle noise. The Bayesian procedure relies on diminishing speckle noise in a preprocessing stage to attain reliable estimates. Also, the Bayesian approach includes a model for speckle noise and therefore can deal with residual speckle noise in a systematic way after the preprocessing stage.

The preprocessing stage is described in Section II-B and roughly consists of averaging pixels (multilooking process) over each field) for an intensity (HH,VV)-pair image until the variance of the backscattering coefficient is not decreased. The statistical properties of the resulting (multilooked) intensity image is described by a bivariate gamma distribution [34, Eq. (30)], i.e.,

$$P^{(n)}_{Z_1Z_2}(z_1,z_2) = \frac{n^{n+1}(z_1z_2)^{(n-1)/2}\exp\left[\dfrac{-n\left(\dfrac{z_1}{C_1}+\dfrac{z_2}{C_2}\right)}{1-\rho^2}\right]}{(C_1C_2)^{(n+1)/2}\Gamma(n)(1-\rho^2)\rho^{n-1}} \times I_{n-1}\left(2n\sqrt{\frac{z_1z_2}{(C_1C_2)}}\frac{\rho}{1-\rho^2}\right) \tag{8}$$

where C_1 and C_2 are the expectation value of Z_1 and Z_2, i.e., $C_1 = E[Z_1]$ and $C_2 = E[Z_2]$, respectively, and are given by means of a forward model which predicts the value of C_1 and C_2 in terms of dielectric constant, roughness, beam incidence angle, and wavelength. In expression (8), n is the number of looks of z_1 and z_2, and ρ is the correlation between z_1 and z_2.

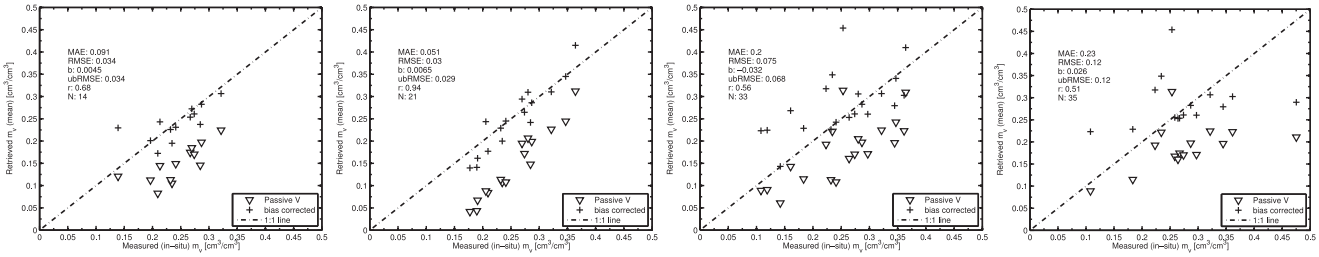

(a) (b) (c) (d)

Fig. 3. Retrieved soil moisture using SCA for V-polarized brightness temperature T_{bV} . A bias correction for surface temperature $T_S^{\rm corr} = 1.10T_S$ is applied. Error metrics correspond to bias-corrected SCAV. (a) 31603. (b) 31604. (c) 31605. (d) 31606.

As mentioned, a forward model maps dielectric constant ε and roughness s, l into the expected value $C = C_i(\varepsilon, s, l; \theta, \lambda)$, $i = 1, 2$. The measured (z_1, z_2) differs from C for several reasons, such as the instrumental errors, the residual speckle after multilooking, and the influence of further soil parameters affecting the radar response, which have not been accounted for in the forward model. Heterogeneities within the radar resolution cell may also represent a source of discrepancy since the forward relation $C(\varepsilon, s, l)$ is non-linear.

C. Bias Correction for Soil Temperature T_S

A bias were found on PALS data when comparing retrieved soil moisture from T_{bV} using SCA to *in situ* soil moisture, as shown in Fig. 3. PALS radiometer calibration stability assured brightness temperature measurements to be within 1 (bias) and 0.2 K (stability) [20]. For typical T_bV values of about 270 K over land, this led to relative errors less than 0.5%. On the other hand, surface soil temperature T_s as required by the $\omega - \tau$ model in (4) is estimated by means of an infrared camera on board the aircraft carrying the PALS. Since the brightness temperature observed at L-band ($\lambda = 23$ cm) originates from a layer of the soil surface whose thickness is several centimeters deep, the soil temperature T_s used to parameterize the $\omega - \tau$ model should account for this extended layer. However, thermal infrared radiation (TIR) as measured by PALS camera is sensitive to the uppermost layer of the soil, known as skin temperature [18]. This skin temperature differs from deeper layers due to thermal inertia of soil. Since PALS acquisitions started around 14:00 h and stopped around 19:00 h, skin layer cooled as the deeper layers heated as heat flowed downwards. Physical temperature at 5 cm depth, measured with *in situ* probes from temporary stations provided by the USDA [18], as underestimated by roughly 10% in the PALS measurements (figure not shown). For this reason, the PALS skin temperature used into SCA caused the bias shown in Fig. 3.

In any case, it was found that the bias shown in Fig. 3 can be corrected adding a 10% to the measured soil temperature, i.e., $T_S^{\rm corr} = 1.10T_S$, where the superscript stands for "corrected." This bias-corrected surface soil temperature was used throughout this study.

Bias can also be corrected by increasing soil roughness. However, it was found that the corrected soil roughness corresponded to RMS heights of about 1.5–2.0 cm, more rough than the commonly accepted value of 1 cm for no-till croplands such as the soybean fields of this study.

D. Soil Dielectric Constant and Volumetric Soil Moisture

The estimator given by expression (2) is an estimator for soil real dielectric constant. However, validation from retrieved estimates is often performed against ground-truth data in terms of volumetric soil moisture m_v. Conversion from real dielectric constant to soil moisture is done by means of a second-order polynomial empirical relationship as stated in [35]. Other dielectric models to convert ε to m_v can be found in [36] and [37]. Hence, inversion to obtain m_v from ε is straightforward

$$m_v = \frac{-b(f,S,C) + \sqrt{b(f,S,C)^2 - 4c(f,S,C)(a(f,S,C) - \varepsilon)}}{2c(f,S,C)} \tag{9}$$

where coefficients a, b, and c depend on frequency f, and S and C are the percentage of sand and clay contained in the soil, respectively. Coefficients for 1.4 and 6 GHz, among others, are explicitly shown in [35, Table II]. Moreover, the error in the estimate m_v can be computed from the error in ε as follows:

$$\text{std}[m_v^{\rm bay}] = \left| \frac{dm_v}{d\varepsilon} \right|_{\varepsilon^{\rm bay}} \text{std}[\varepsilon^{\rm bay}] \tag{10}$$

where $\text{std}[m_v^{\rm bay}]$ is the error computed as the standard deviation of the soil moisture estimator and the total derivative is readily computed from (9) and is evaluated at $\varepsilon^{\rm bay}$.

E. Total Error in Field-Based in situ Soil Moisture

Portable impedance probes measure the dielectric properties of the soil–water–air mixture from which the volumetric soil moisture can be inferred. The instrument error after performing a field-specific calibration is [15]

$$e_{\rm inst} = \sqrt{e_{\rm bias}^2 + \frac{e_{\rm rmse}^2}{M}} \tag{11}$$

where M is the number of measurement replicates ($M = 3$), $e_{\rm bias}$ and $e_{\rm rmse}$ are the bias (which refers to the accuracy) and the statistical error (which refers to the precision) of the linear fitting among the volumetric water content using gravimetric (oven-dry) method for core samples and the calculated volumetric water content using the field-specific calibration for the probes.

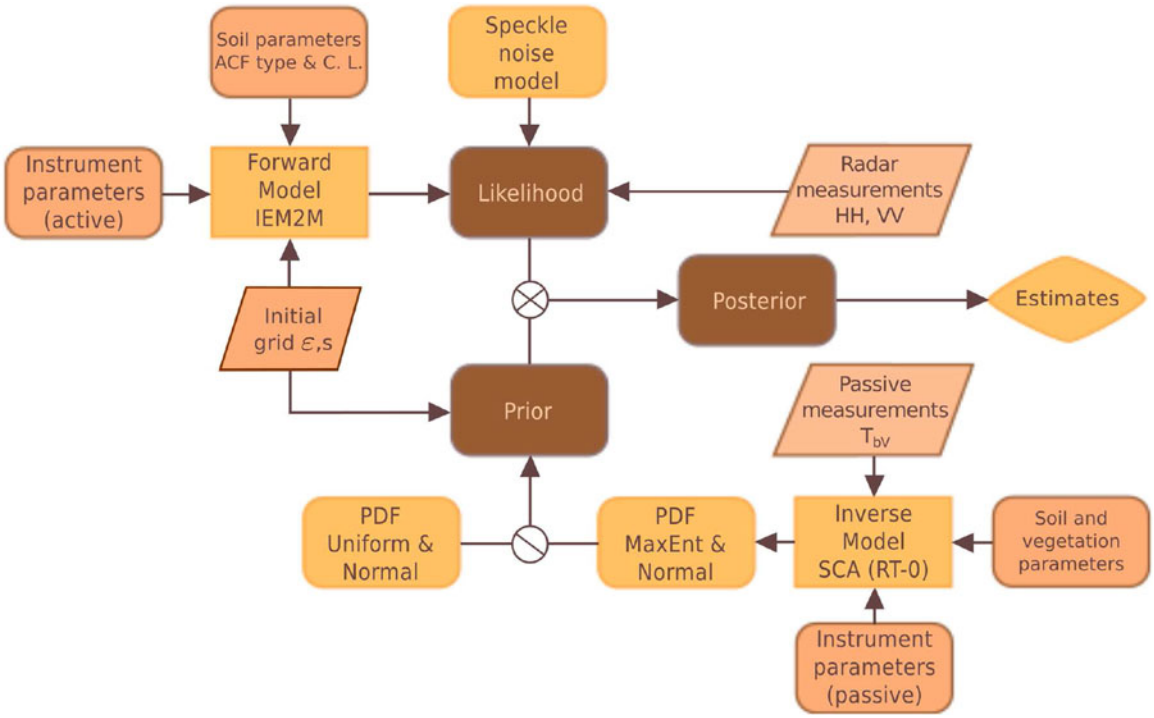

Fig. 4. Flowchart of the B-CAP retrieval scheme. Symbol of a cross mark encircled indicates product operation. Single line encircled indicates an 'Or' statement.

For the SMAPVEx12 campaign, such a calibration yielded a negligible bias and a statistical error ranging from 0.012 to 0.054 cm^3/cm^3 for the soybean fields analyzed here [38, Table 2]. In addition to instrument errors, a second error source comes from the spatial variability of the soil moisture at field size S, quantified by the standard deviation $\sigma(m_v^S)$ [14]. An error estimate σ_S for the true field-mean soil moisture m_v computed from N sparse site measurements over the field extent is given by [39, Ch. 7]

$$\sigma_S = \frac{\sigma(m_v^S)}{\sqrt{N}} t_{\frac{\alpha}{2},N-1} \tag{12}$$

where $t_{\frac{\alpha}{2},N-1}$ is the α quantile of the Student's t distribution with $N-1$ degrees of freedom. Expression (12) defines a $100\alpha\%$ confidence region for the true mean value m_v. In (12), the standard deviation of soil moisture at field size S is computed as [14], [15]

$$\sigma(m_v^S) = \frac{S^{\frac{D}{2}}}{X_0^D} \tag{13}$$

where $D = 0.086$, $X_0 = 2.879 \times 10^{17}$ m, and S is the spatial scale on which soil moisture is retrieved. Thus, S is the size of each field (i.e., 800 m by 800 m or 6.4×10^5 m^2), since this paper deals with field-based retrieved estimates.

The standard deviation allowed by expression (13) has a dynamic range of 0.040 cm^3/cm^3 for the spatial scale $S_l = 256$ m^2 to 0.059 cm^3/cm^3 for the spatial scale $S_u = 2.56$ km^2 [14]. S_l and S_u are the lower and upper spatial scales corresponding to the feasible region in (13), respectively.

TABLE I
COMPONENTS AND TOTAL ERROR FOR IN SITU SOIL MOISTURE FOR EACH SITE

Field	e_{inst} [cm^3/cm^3]	σ_S [cm^3/cm^3]	e_{grd} [cm^3/cm^3]
14	0.012	0.055	0.056
33	0.047	0.055	0.062
63	0.034	0.055	0.058
64	0.027	0.055	0.057
82	0.040	0.055	0.060
103	0.038	0.055	0.060
111	0.043	0.055	0.061
113	0.040	0.055	0.060
114	0.044	0.055	0.061
123	0.054	0.055	0.064

Finally, the total error e_{grd} in the ground estimate is

$$e_{\text{grd}} = \sqrt{e_{\text{inst}}^2 + \sigma_S^2} \tag{14}$$

where e_{inst} is the total instrument error and σ_S is the uncertainty related to the spatial variability of the soil moisture at extent S. Numerical evaluation of (11), (13), and (14) is shown in Table I.

The *in situ* soil moisture estimates shown in Section V have error bars computed from (14).

F. Flowchart of the Methodology

A flowchart of the procedure adopted in this paper is shown in Fig. 4. The electromagnetic forward model describes, at a certain level of accuracy, the interaction of the radar pulse with the soil and predicts how this amount of energy is modified by the dielectric and geometric properties of the target in his way back to the

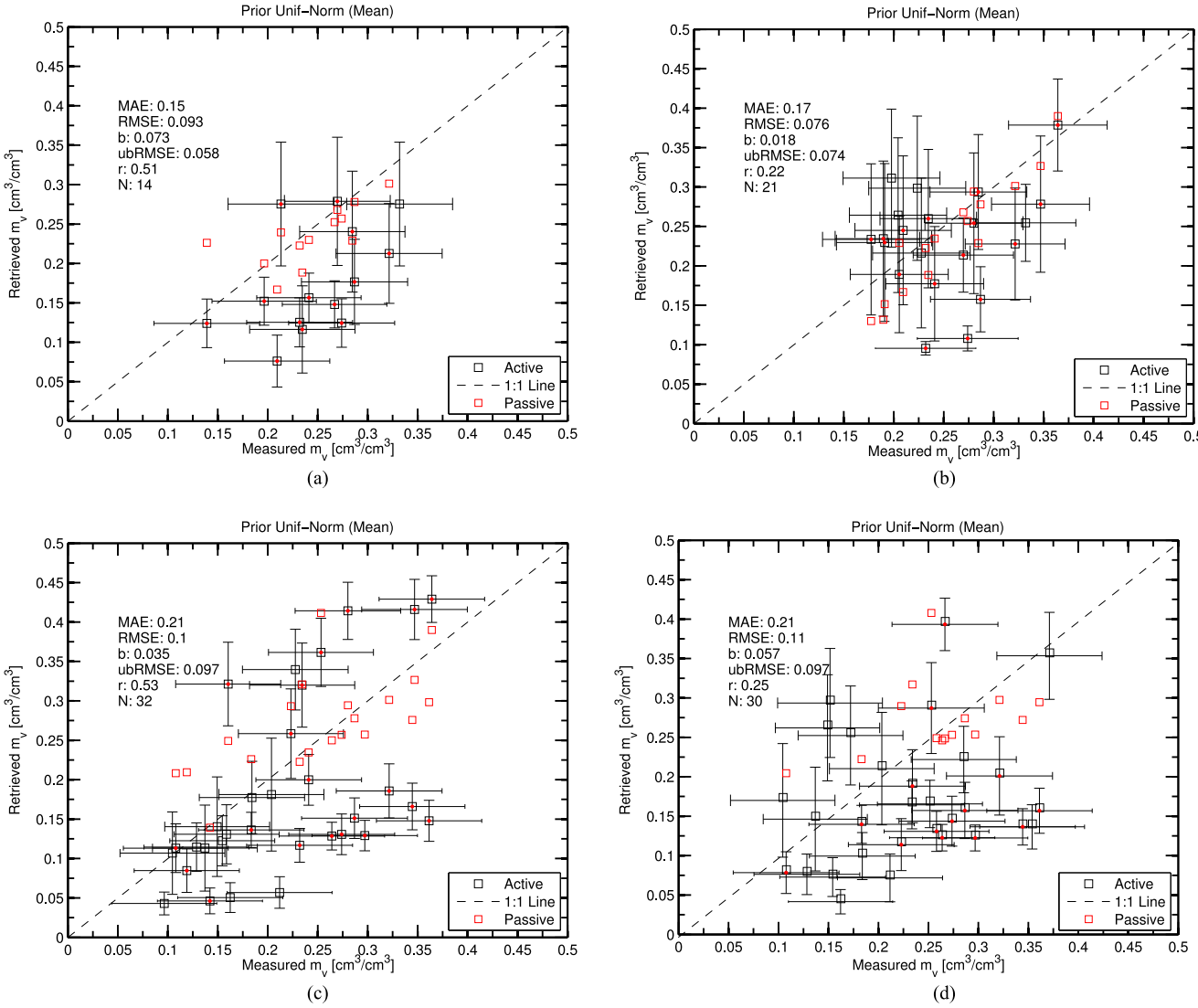

Fig. 5. Retrieved estimates for volumetric soil moisture m_v against measured ground-truth data for bare or sparsely-vegetated soil (RVI < 0.3). Uniform prior $P_\varepsilon \sim U(3, 30)$ for dielectric constant ε and Normal prior $P_S \sim N(\mu_s, \sigma_s)$ for RMS height s, with the mean μ_s determined by the ground-truth data were used. The four flight lines are displayed: (a) 31603, (b) 31605, (c) 31605, and (d) 31606. Error metrics correspond to only active retrieval. Error metrics for bias-corrected passive are shown in Fig. 3.

sensor. This depends on soil and system parameters. The integral equation model with multiple scattering at second order, named as IEM2M [16], is the rigorous forward model adopted in this paper. An initial grid of dielectric constant ε and RMS height s is used to generate outputs for HH and VV co-polarized intensity images. The Bayesian approach includes a model for speckle noise and therefore can deal with the residual speckle noise after multilooking in a systematic way. The statistical properties of two multilooked intensity images are described by a bivariate gamma $P_{\mathrm{HHVV}}(hh, vv|C_{\mathrm{HH}}, C_{\mathrm{VV}}, n, \rho)$ [34, Eq. (30)], where C_{HH} and C_{VV} are the predicted (expected) values of the forward model, n is the number of looks, and ρ is the correlation between HH and VV. The likelihood function is then constructed on evaluating the distribution P_{HHVV} on the measured backscattering coefficient $\mathrm{HH}_{\mathrm{meas}}$ and $\mathrm{VV}_{\mathrm{meas}}$ after multilooking, i.e., $P_{\mathrm{HHVV}}(\mathrm{HH}_{\mathrm{meas}}, \mathrm{VV}_{\mathrm{meas}}|C_{\mathrm{HH}}, C_{\mathrm{VV}}, n, \rho)$. The posterior is the product of the likelihood function by the prior distribution. Dielectric constant estimates are computed from the posterior distribution as above mentioned, and then converted into soil moisture using the empirical relationship from [35] described in Section IV-D.

V. Results

Retrieved estimates for volumetric soil moisture m_v against measured ground-truth data are shown in Fig. 5 for the four flight lines described in Section II-A. The black squares are the estimates from the radar (active) HH- and VV-measurements using priors uniform and normal for ε and s, respectively. The red squares indicate estimates from passive microwave data independently of the radar estimation. (Brightness temperature were partly available for the entire radar dataset.) Red points within black markers indicate that passive microwave-based soil

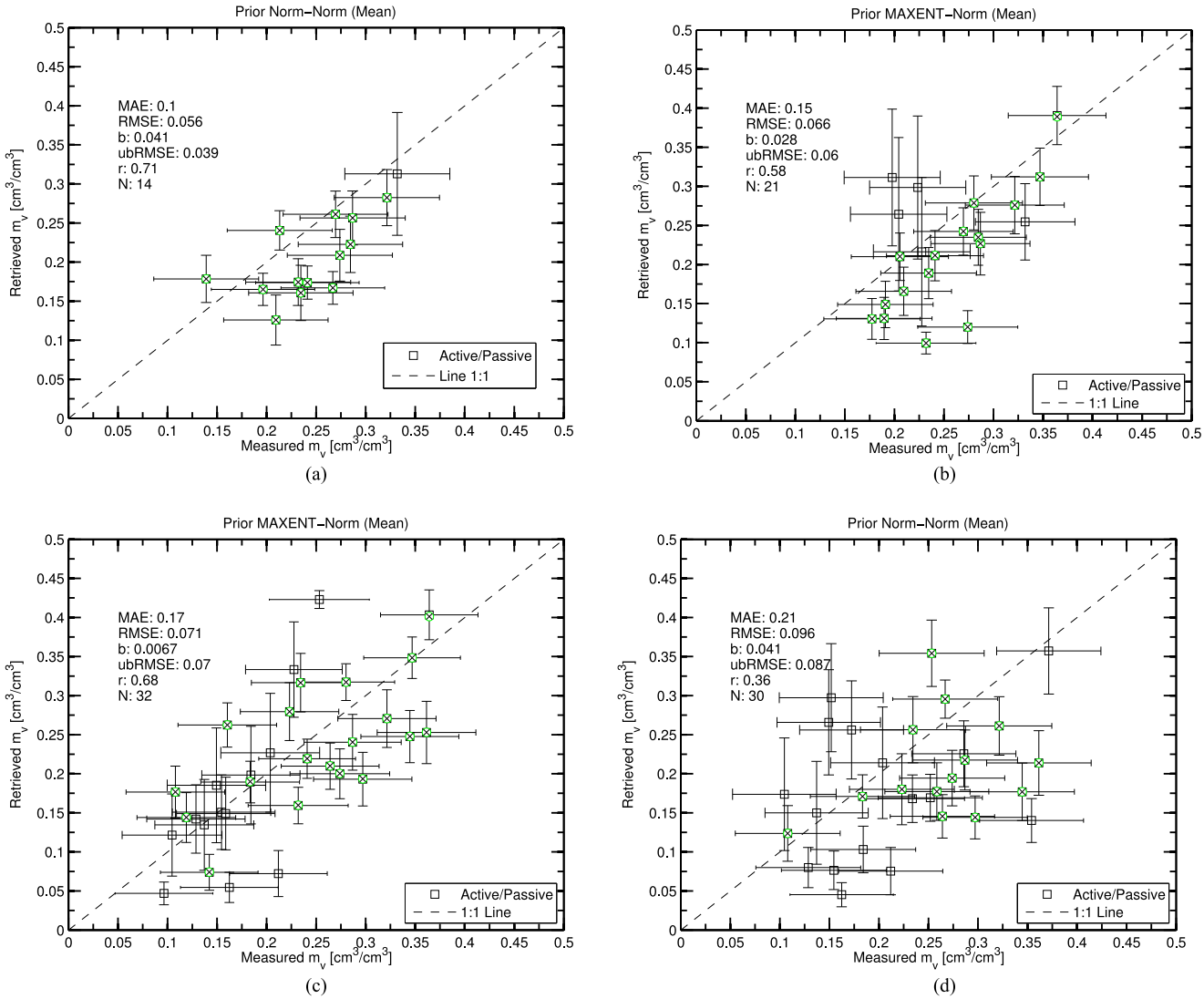

Fig. 6. Retrieved estimates for volumetric soil moisture m_v against measured ground-truth data for bare or sparsely-vegetated soil (RVI < 0.3). Max Ent prior for ε with μ_ε given by the SCA retrieval algorithm and Normal prior $P_S \sim N(\mu_s, \sigma_s)$ for RMS height s, with the mean μ_s determined by the ground-truth data were used. The four flight lines are displayed: (a) 31603, (b) 31605, (c) 31605, and (d) 31606.

moisture guess is available. Error bars in ground-truth data are computed as mentioned in Section IV-E and accounted for the instrument error (dielectric probe) and the ground-based soil moisture variability. Error bars in the retrieval estimate are related to the spread of the posterior, which in turn is related to the residual speckle noise and the heterogeneity of the scatter.

Retrieved estimates that underestimate measured m_v can be related to an overestimation of the IEM2M model, causing that lower values of m_v matched the observed backscattering coefficient. For instance, cluster of points around measured 0.15 and 0.30 cm^3/cm^3 in Fig. 5(c) can be traced to sites 63, and 111 and 113, respectively [see Fig. 2(c)]. A similar statement holds for an overestimation in retrieved soil moisture and an underestimation in backscattering coefficients by the IEM2M. Error metrics indicate a poor retrieval performance with RMSE around 0.08–0.11 cm^3/cm^3 and a correlation coefficient at most $r = 0.53$. MAE is the most evident error metric for tracing back model misestimations. MAE has values as large as 0.21 cm^3/cm^3, indicating a poor agreement with the forward model.

In Fig. 6, the CAP estimates are shown. Crosses onto green circles indicate radar estimates enhanced by passive measurements, where the Uniform prior was replaced by a MaxEnt one with mean value given by the dielectric constant estimate from SCA. The CAP estimation shows an overall well agreement with an rmse $=$ 0.06–0.07 cm^3/cm^3 and a higher sensitivity with correlation coefficient $r \sim 0.6 - 0.7$ for datasets 31603–31605. Retrieval performance of dataset 31606 is poorer since a large amount of measurements had not their passive counterpart. It is worth mentioning that combined retrieval performs better also than only bias-calibrated passive retrieval. This could be seen from comparing the error metrics from Figs. 3 and 6.

Finally, to assess the performance of the B-CAP algorithm for each location, results on a time series basis are shown in Fig. 7. The retrieval generally performed with an rmse

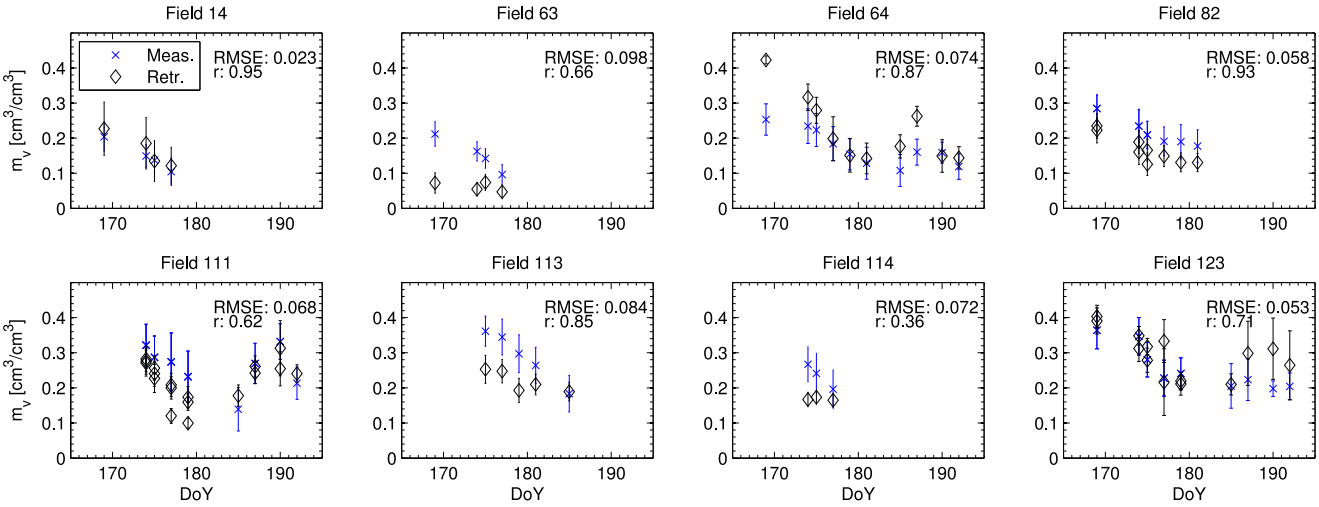

Fig. 7. Time series of the measured (*in situ*) estimates and the CAP retrieved estimates for soil moisture versus the day of the year (DoY).

$\lesssim 0.07\,\mathrm{cm}^3/\mathrm{cm}^3$ and a correlation $r \gtrsim 0.6$ except for the fields 63, 113, and 114. For fields 63 and 113, retrieved soil moisture overestimation is expected from model simulation comparison, as described in Section II-B. The low value of r for field 114 can be ascribed to the low amount of measurements.

VI. Conclusion

When remotely sensed active and passive microwave observations are available at similar extents, a Bayesian merging technique can be used to retrieve radar soil moisture estimations constrained by a preliminary soil moisture guess from passive microwave observations. In addition, soil moisture retrieved on an field basis minimize errors due to uncertainties in soil roughness.

A complete dataset containing backscattering coefficients and brightness temperatures were used to test the B-CAP retrieval algorithm using HH, VV, and T_{bV}. The dataset is based on a field experiment over bare and sparsely-vegetated soils (RVI < 0.3), covering a wide range of moisture and roughness conditions, which turned it suitable for validation purposes. A bias correction was performed on PALS infrared sensor adding a 10% to the measured surface temperature, thus, compensating a systematic uncertainty. No further calibration was required for the SAR sensor on UAVSAR. Nonetheless, the forward model did overestimate or underestimate the observed backscattering coefficients. This can be related to the presence of developing vegetation, wet stubble, or crop rows, the features not modeled by the forward model IEM2M.

Yet, an overall improvement of the radar prediction on field-based soil moisture were achieved by including information from passive microwaves. Comparison were done by taking into account soil moisture uncertainties that involves soil moisture variability and dielectric probe error. Performance metrics are used to assess the retrieval methodology. Agreement ranges from 0.08 to 0.11 $\mathrm{cm}^3/\mathrm{cm}^3$ for only active and improves to 0.06–0.10 $\mathrm{cm}^3/\mathrm{cm}^3$ for the combined technique. It is worth mentioning that the active dataset has only partially its passive counterpart. The combined technique also showed a better clustering of the data along the 1:1 line, highlighting the improvement on sensitivity of the soil moisture estimates. By analyzing the time series for each field, an RMSE less than 0.07 $\mathrm{cm}^3/\mathrm{cm}^3$ and a correlation coefficient r larger than 0.6 were found providing the forward model is accurate enough. Thus, this paper contributed to demonstrate that the active/passive synergy can produce an enhanced soil moisture product, with a better performance than each one separately. The B-CAP algorithm can exploit ongoing ALOS-2 mission and planned SAOCOM mission for the radar observations, and SMAP mission for the radiometer ones.

References

[1] D. Entekhabi *et al.*, "The soil moisture active passive (SMAP) mission," *Proc. IEEE*, vol. 98, no. 5, pp. 704–716, May 2010.

[2] A. Moreira *et al.*, "Tandem-L: A highly innovative bistatic SAR mission for global observation of dynamic processes on the earth's surface," *IEEE Geosci. Remote Sens. Mag.*, vol. 3, no. 2, pp. 8–23, Jun. 2015.

[3] C. Oliver and S. Quegan, *Understanding Synthetic Aperture Radar Images*. Raleigh, NC, USA: SciTech Publishing, 2004.

[4] N. E. C. Verhoest, H. Lievens, W. Wagner, J. Alvarez-Mozos, M. S. Moran, and F. Mattia, "On the soil roughness parameterization problem in soil moisture retrieval of bare surfaces from synthetic aperture radar," *Sensors*, vol. 8, pp. 4213–4248, Jul. 2008.

[5] N. N. Das, D. Entekhabi, E. G. Njoku, J. J. C. Shi, J. T. Johnson, and A. Colliander, "Tests of the SMAP combined radar and radiometer algorithm using airborne field campaign observations and simulated data," *IEEE Trans. Geosci. Remote Sens.*, vol. 52, no. 4, pp. 2018–2028, Apr. 2014.

[6] C. Notarnicola and F. Posa, "Bayesian algorithm for the estimation of the dielectric constant from active and passive remotely sensed data," *IEEE Geosci. Remote Sens. Lett.*, vol. 1, no. 3, pp. 179–183, Jul. 2004.

[7] F. Mattia, G. Satalino, L. Dente, and G. Pasquariello, "Using *a priori* information to improve soil moisture retrieval from ENVISAT ASAR AP data in semiarid regions," *IEEE Trans. Geosci. Remote Sens.*, vol. 44, no. 4, pp. 900–912, Apr. 2006.

[8] N. N. Das, D. Entekhabi, and E. G. Njoku, "An algorithm for merging SMAP radiometer and radar data for high-resolution soil-moisture retrieval," *IEEE Trans. Geosci. Remote Sens.*, vol. 49, no. 5, pp. 1504–1512, May 2011.

[9] D. Entekhabi, N. Das, E. Njoku, S. Yueh, J. Johnson, and J. Shi, "SMAP algorithm theoretical basis document L2 & L3 radar/radiometer soil moisture (active/passive) data products," Revision A, Jet Propulsion Laboratory, California Institute of Technology, Dec. 9, 2014.

[10] D. J. Leroux *et al.*, "Active-passive soil moisture retrievals during the SMAP validation experiment 2012," *IEEE Geosci. Remote Sens. Lett.*, vol. 13, no. 4, pp. 475–479, Apr. 2016.
[11] R. Akbar and M. Moghaddam, "Radar-radiometer soil moisture estimation with joint physics and adaptive regularization in support of SMAP," in *Proc. 2014 IEEE Int. Geosci. Remote Sens. Symp.*, Jul. 2014, pp. 3634–3637.
[12] U. Narayan, V. Lakshmi, and T. J. Jackson, "High-resolution change estimation of soil moisture using l-band radiometer and radar observations made during the SMEX02 experiments," *IEEE Trans. Geosci. Remote Sens.*, vol. 44, no. 6, pp. 1545–1554, Jun. 2006.
[13] A. Colliander *et al.*, "Retrieving soil moisture for non-forested areas using PALS radiometer measurements in SMAPVEX12 field campaign," *Remote Sens. Environ.*, vol. 184, pp. 86–100, 2016.
[14] J. S. Famiglietti, D. Ryu, A. A. Berg, M. Rodell, and T. J. Jackson, "Field observations of soil moisture variability across scales," *Water Resour. Res.*, vol. 44, no. 1, 2008, Art. no. W01423.
[15] M. Barber, F. Grings, C. Bruscantini, and H. Karszenbaum, "Rationale behind an optimal field experiment to assess the suitability of soil moisture retrieval algorithms for SAR data," *IEEE Geosci. Remote Sens. Lett.*, vol. 12, no. 4, pp. 791–795, Apr. 2015.
[16] J. L. Álvarez-Pérez, "The IEM2M rough-surface scattering model for complex-permittivity scattering media," *Waves Random Complex Media*, vol. 22, no. 2, pp. 207–233, 2012.
[17] "SMAP Validation Experiment 2012, Experimental Plan," [Online]. Available: https://smapvex12.espaceweb.usherbrooke.ca
[18] H. McNairn *et al.*, "The soil moisture active passive validation experiment 2012 (SMAPVEx12): Prelaunch calibration and validation of the smap soil moisture algorithms," *IEEE Trans. Geosci. Remote Sens.*, vol. 53, no. 5, pp. 2784–2801, May 2015.
[19] A. G. Fore *et al.*, "UAVSAR polarimetric calibration," *IEEE Trans. Geosci. Remote Sens.*, vol. 53, no. 6, pp. 3481–3491, Jun. 2015.
[20] "SMAPVEX12 PALS Backscatter Data Documentation," http://nsidc.org/data/docs/daac/smap/smapvex12/sv12plbk/index.html
[21] M. Barber, M. Maas, P. Perna, F. Grings, and H. Karszenbaum, "A Bayesian approach to retrieve soil parameters from SAR data: Effect of prior information," *Proc. SPIE*, vol. 8536, 2012, Art. no. 85360N.
[22] D. Entekhabi, R. H. Reichle, R. D. Koster, and W. T. Crow, "Performance metrics for soil moisture retrievals and application requirements," *J. Hydrometeorol.*, vol. 11, no. 3, pp. 832–840, 2010, doi: 10.1175/2010JHM1223.1
[23] T. Jackson, T. Schmugge, and J. Wang, "Passive microwave sensing of soil moisture under vegetation canopies," *Water Resour. Res.*, vol. 18, no. 4, pp. 1137–1142, 1982.
[24] X. Zhan, P. R. Houser, J. P. Walker, and W. T. Crow, "A method for retrieving high-resolution surface soil moisture from hydros l-band radiometer and radar observations," *IEEE Trans. Geosci. Remote Sens.*, vol. 44, no. 6, pp. 1534–1544, Jun. 2006.
[25] T. Jackson, "III. measuring surface soil moisture using passive microwave remote sensing," *Hydrol. Process.*, vol. 7, no. 2, pp. 139–152, 1993.
[26] E. T. Jaynes and G. L. Bretthorst, Eds.,*Probability Theory: The Logic of Science*. Cambridge, U.K.: Cambridge Univ. Press, 2003.
[27] A. K. Fung, *Microwave Scattering and Emission Models and Their Applications* (The Artech House Remote Sensing Library). Norwood, MA, USA: Artech House, 1994.
[28] J. A. Ogilvy, *Theory of Wave Scattering from Random Rough Surfaces*. Bristol, U.K.: IOP Publishing Ltd., 1991.
[29] L. Tsang, J. A. Kong, and K. Ding, *Scattering of electromagnetic waves: Theories and Applications*, vol. 1. New York, NY, USA: Wiley, 2000.
[30] A. K. Fung and K. S. Chen, *Microwave Scattering and Emission Models for Users*. Norwood, MA, USA: Artech House, 2010.
[31] Y. Kim, T. Jackson, R. Bindlish, Hoonyol Lee, and S. Hong, "Radar vegetation index for estimating the vegetation water content of rice and soybean," *IEEE Geosci. Remote Sensing Lett.*, vol. 9, no. 4, pp. 564–568, Jul. 2012.
[32] M. Zribi *et al.*, "Backscattering behavior and simulation comparison over bare soils using SIR-C/X-SAR and ERASME 1994 data over ORGEVAL," *Remote Sens. Environ.*, vol. 59, no. 2, pp. 256–266, 1997.
[33] F. Mattia *et al.*, "The effect of surface roughness on multifrequency polarimetric SAR data," *IEEE Trans. Geosci. Remote Sens.*, vol. 35, no. 4, pp. 954–966, Jul. 1997.
[34] J. S. Lee, K. W. Hoppel, S. A. Mango, and A. R. Miller, "Intensity and phase statistics of multilook polarimetric and interferometric SAR imagery," *IEEE Trans. Geosci. Remote Sens.*, vol. 32, no. 5, pp. 1017–1028, Sep. 1994.
[35] M. T. Hallikainen, F. T. Ulaby, M. C. Dobson, M. A. El-Rayes, and L.-K. Wu, "Microwave dielectric behavior of wet soil-Part I: Empirical models and experimental observations," *IEEE Trans. Geosci. Remote Sens.*, vol. GE-23, no. 1, pp. 25–34, Jan. 1985.
[36] N. R. Peplinski, F. T. Ulaby, and M. C. Dobson, "Dielectric properties of soils in the 0.3-1.3-GHz range," *IEEE Trans. Geosci. Remote Sens.*, vol. 33, no. 3, pp. 803–807, May 1995.
[37] V. L. Mironov, M. C. Dobson, V. H. Kaupp, S. A. Komarov, and V. N. Kleshchenko, "Generalized refractive mixing dielectric model for moist soils," *IEEE Trans. Geosci. Remote Sens.*, vol. 42, no. 4, pp. 773–785, Apr. 2004.
[38] "SMAPVEX12 Hydra Theta Probe Calibration," [Online]. Available: https://smapvex12.espaceweb.usherbrooke.ca/Hydra_Theta_Probe_Calibration_final.pdf, 12 2012.
[39] K. Knight, *Mathematical Statistics* (Chapman & Hall/CRC Texts in Statistical Science Series). London, U.K.: Chapman & Hall/CRC Press, 2000.

Matias Barber (M'11) received the M.S. degree in physics from the University of Buenos Aires, Buenos Aires, Argentina, in 2009 and the Ph.D. degree in physics from the same university in 2014.

He joined the National Scientific and Technical Research Council as an Assistant Researcher in 2015, working at Quantitative Remote Sensing Group, Institute of Astronomy and Space Physics, Buenos Aires, Argentina. He was involved in airborne instrument campaigns and is currently working on an alternative soil moisture retrieval algorithm to be used in the L-band full polarimetric SAOCOM mission from the National Commission for Space Activities, Argentina. His research interests include polarimetry and wave scattering.

Cintia Bruscantini (M'15) received the Ph.D. degree in engineering from the University of Buenos Aires, Buenos Aires, Argentina, in 2016.

She is an Electronic Engineer and holding a Post-Doc Position in the Quantitative Remote Sensing Group, Institute of Astronomy and Space Physics, Buenos Aires, Argentina. Her research interests include Observing System Simulation Experiment, Bayesian inference, and hardware development. She has collaborated with the National Commission for Space Activities, Argentina for the calibration of the microwave radiometer on board the Aquarius/SAC-D.

Francisco Grings received the M.S. degree in medical physics from the University of San Martin, Buenos Aires, Argentina, in 2003 and the Ph.D. degree in physics from the University of Buenos Aires, Buenos Aires, Argentina, in 2008.

He is a Physicist and an Independent Researcher Member of the National Scientific and Technical Research Council, working in the Institute of Astronomy and Space Physics (IAFE), Buenos Aires, Argentina.

He is responsible of IAFEs Quantitative Remote Sensing Group. He is leading the Observing System Simulation Experiment project at IAFE, which includes model simulations and proofs of concepts of future spaceborne remote sensing instruments.

Haydee Karszenbaum (M'15) received the M.S. degree in physics from the University of Tennessee, Knoxville, TN, USA, in 1970.

She was a Research Fellow at College of Marine Studies, University of Delaware, Newark, DE, USA. Since the 1980s, she has a Research Member of National Scientific and Technical Research Council, a remote sensing specialist, and the Director of the Quantitative Remote Sensing Group, Institute of Astronomy and Space Physics, Buenos Aires, Argentina. She has been involved since more than two decades with the Argentine Space Program through National Commission for Space Activities AO projects and technology transfer agreements. She is currently the PI of national projects. Her main interest focuses on microwave remote sensing applied to agriculture, hydrology, and climatic studies.